RSC Advances

PAPER

View Article Online
View Journal | View Issue

Cite this: *RSC Adv.*, 2020, **10**, 16576

Electrodeposition of nickel in air- and water-stable 1-butyl-3-methylimidazolium dibutylphosphate ionic liquid

Yu Zheng,[ab] Xiaorong Zhou,*[b] Yunbai Luo [a] and Ping Yu *[a]

Received 13th January 2020
Accepted 20th April 2020

DOI: 10.1039/d0ra00351d

rsc.li/rsc-advances

Nickel coating was obtained by potentiostatic electrodeposition in 1-butyl-3-methylimidazolium diethylphosphate ionic liquid without any additive. Further, cyclic voltammetry (CV) tests were used to investigate the electrochemical behaviour of Ni^{2+} in the ionic liquid, revealing that the electrodeposition of nickel in this ionic liquid is an irreversible process. It was revealed that the diffusion of Ni^{2+} is a rate-determining step in the electrodeposition process. Further, the influence of dissolved water and applied voltage on electrodeposition were also studied using scanning electron microscopy (SEM).

Introduction

Last century, ionic liquids (ILs) were developed when researchers were looking for electrolytes for batteries.[1] ILs are, generally, composed of cations and anions, with a melting point below 373 K, thus, they are also known as room temperature molten salts.[2] Because of their unique structures, ILs have many attractive properties, such as high conductivity, large electrochemical potential windows, good thermal stability, non-volatility and non-toxicity. Thus, ILs are used for electrochemical devices, electroplating of metals and organic synthesis. Traditionally, electrochemical processes take place in aqueous electrolytes, while the relatively narrow electrochemical potential window of water is a major limitation, especially for electrodeposition of some metals with relatively negative redox potential.[3] The large electrochemical potential window of ILs means much wider redox potential, which makes it possible to electrodeposit reactive metals. For example, Winnick *et al.* electrodeposited sodium in a 1-ethyl-3-methylimidazolium chloride/aluminum chloride-based system.[4] In recent years, significant attention is paid to electrodeposition of various metals in ILs since anions and cations can be designed to modify coating properties including Fe,[5–7] Ni,[8–13] Co,[10,14] Cu,[15–17] Ag,[18,19] Au,[19] Al[19–24] and Ce[16] coatings.

Electrodeposition of nickel is widely used to obtain metallic nickel coatings for corrosion protection and decoration.[25–27] Currently, the dominant commercial nickel electroplating processes are based on Watts nickel bath developed by Oliver P. Watts in 1916 which is used to produce bright, dark, hard nickel coating and so on for different applications.[28] Further, the morphology and properties of the coatings obtained from Watts bath can be controlled by organic and inorganic additives in the bath.[29] However, despite its wide use, alternative method is sought by electroplating industry since Watts bath also brings about many issues, including, firstly, hydrogen evolution during the electroplating process, which has two major negative impacts, reducing current efficiency and compromising the quality of resultant coatings; secondly, pollution associated with Watts bath.[25]

In recent years, electrodeposition of nickel in air- and water-stable ionic liquids is a focus of research. Ming-Jay Deng investigated the electrodeposition of nickel on copper in 1-ethyl-3-methylimidazolium-dicyanamide by potentiostatic process and found that the morphology of nickel coating depends on deposition potential.[30] Yan-Li Zhu studied the electrochemical behavior of Ni^{2+} during electrodeposition of nickel in butyl-1-methylpyrrolidinium bis(trifluoromethylsulfonyl)amide (BMPTFSA).[31] More recently, researchers successfully achieved electrodeposition of nickel in eutectic-based ionic liquid. Andrew P. Abbott compared the difference of nickel coatings deposited in aqueous solution and eutectic-based ionic liquid and found that the nickel coating obtained from eutectic-based ionic liquid has harder and flatter surface; furthermore, with molecule additives he obtained bright nickel coating from eutectic-based ionic liquid.[25,26] B. Meenatchi investigated electrodeposited of nickel from protic ionic liquids with imidazolium cation without additives, while morphology of nickel coatings are sponge and gravel-like.[32] Despite extensive research on electrodeposition of nickel and other metals from ILs, there are still many issues limiting their wide application. Firstly, many ILs are sensitive to water and air, which means that electrodeposition process in these ILs needs to be conducted in glove boxes, therefore, are not suitable for large scale application. Secondly, both quality and variety of electrodeposited nickel coating from ILs can't fully meet the

[a]College of Chemistry and Molecular Sciences, Wuhan University, Wuhan 430072, Hubei, People's Republic of China. E-mail: yuping@whu.edu.cn

[b]Corrosion and Protection Centre, School of Materials, The University of Manchester, The Mill, Sackville St, Manchester, M13 9PL, UK. E-mail: xiaorong.zhou@manchester.ac.uk

requirements of application. Thus, further research is still needed in electrodeposition of nickel in ILs, especially on developing air- and water-stable ILs which are suitable for producing high quality nickel coatings.

In a previous study by the authors, it was found that ionic liquid—1-butyl-3-methylimidazolium diethylphosphate ([BMIM][DBP]) (the chemical structural is shown in Fig. 1) is an air- and water-stable ionic liquid with attractive properties, such as low cost, designable pH value and low toxicity.[33] In the present work electrodeposition of nickel in [BMIM][DBP] without additive is investigated with focus on the electrochemical behavior of Ni^{2+} in [BMIM][DBP], the electrodeposition mechanism, the influence of water content and applied voltage on the morphology of the resultant nickel coating.

Experimental section

Chemicals

Ionic liquid [BMIM][DBP] (chemical structure is shown in Fig. 1) was synthesized in laboratory. *N*-Methylimidazole (82.1 g, 1 mol) was added dropwise to a 500 mL flask containing 266.3 g (1 mol) tributylphosphate at 423 K, and the liquid was stirred at this temperature for 5 h. Then, the mixture was transferred to a 500 mL beaker that was, then, kept in a vacuum oven maintained at 420 K under 5 mmHg for 7 days to remove residual reactant. Finally, the [BMIM][DBP] product was collected in a container and stored in clean and dry environment. $NiCl_2$ ionic liquid solution was prepared by stirring the mixture of $NiCl_2 \cdot 6H_2O$ and the [BMIM][DBP] until a homogeneous green liquid was formed.

Electrochemical experiments

All electrochemical experiments, including cyclic voltammetry and electrodeposition, were performed in a three-electrode cell, where a silver wire was used as the quasi-reference electrode; platinum was used as the counter electrode and copper sheet was used as working electrode. Copper substrate was, firstly, grinded with silicon carbide papers and washed with distilled water, ethanol and acetone in sequence. After grinding, copper substrate was polished with 1 μm and 0.4 μm polishing paste sequentially to obtain a mirror finish. Finally, the copper electrode was sealed by polyimide tapes leaving a working area of 10 mm × 10 mm. Electrochemical experiments were carried out using a CHI660E electrochemical workstation (CH Instruments, Inc).

Characterization of resultant coatings

After electrodeposition, the specimens were cleaned in acetone, and dried in air. The resultant coatings were characterized using scanning electron microscopy (Zesis Ultra 55) and X-ray diffraction (XRD, Shimadzu XRD-6100). A Keyence X200K 3D laser microscope was used to characterize surface morphology of the coatings.

Result and discussion

Cyclic voltammetry

In order to exclude the influence of water, anhydrous $NiCl_2$ was used for preparing 0.1 M anhydrous $NiCl_2$/[BMIM][DBP] for cyclic voltammetry (CVs) at 333 K. CV was conducted by scanning from open circuit potential (OCP) negatively to −0.7 V (*vs.* Ag), followed by a reversed scan back to OCP with various scan rates as presented in Fig. 2. It is evident that at initial stage current densities slightly increase (the minus sign in front of current densities means cathodic current). At potential around −0.35 V (*vs.* Ag) current densities dramatically increase until reach maximum current then decrease, exhibiting a current peak on each curve with different scan rate. At initial stage, the potential is more positive than the reduction potential of Ni^{2+}, thus, only nonfaradaic currents (mainly double-layer charging current) were recorded.[34] When the electrode potential reaches −0.35 V (*vs.* Ag) reduction of Ni^{2+} begins. As indicated by the Butler–Volmer equation current density increases with overpotential, thus, at this stage reduction current rises dramatically with overpotential.[33] As Ni^{2+} ions are reduced at the electrode surface, Ni^{2+} concentration drops progressively, creating a concentration gradient between the electrode surface and the bulk solution, which leads to diffusion of Ni^{2+} from

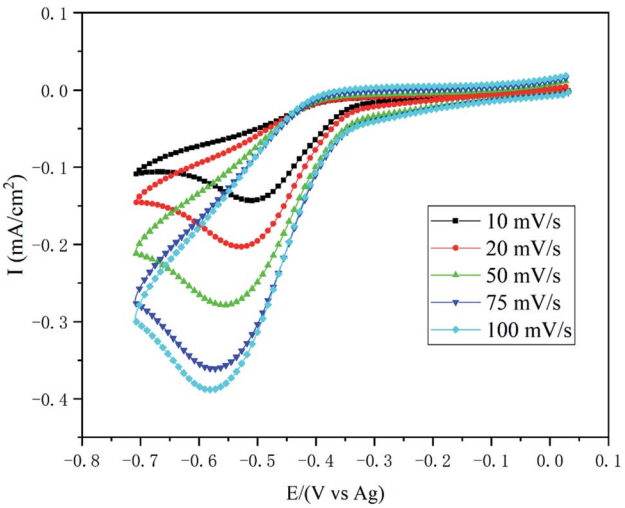

Fig. 2 Cyclic voltammograms of Cu electrodes in 0.1 M $NiCl_2$/[BMIM][DBP] at various scan rate.

Fig. 1 The chemical structure of [BMIM][DBP].

bulk solution towards the electrode surface. When Ni^{2+} ions reduction rate is equal to that of diffusion. The reduction reaction rate reaches maximum as the control step is switch from activation polarization to diffusion polarization. With further increase of overpotential, the current decrease due to the depletion effect, thus a peaked current–potential curve is observed.[34]

Comparing the current peaks at various scan rates, it is evident that with the rise of scan rate the peak current potential (E_p) shifts negatively and the value of peak current (I_p) increases, indicating that the reduction of nickel in this ionic liquid is an irreversible electrochemical process.[34] For irreversible electrode reaction, the relationship between the E_p and scan rates ($v^{1/2}$) can be described by eqn (1).[35–37]

$$E_p = E^{\ominus'} - \frac{RT}{\alpha F}\left[0.780 + \ln\left(\frac{D^{\frac{1}{2}}}{k^0}\right) + \ln\left(\frac{\alpha F}{RT}\right)^{\frac{1}{2}}\right] - \frac{RT}{\alpha F}\ln v^{1/2} \quad (1)$$

where $E^{\ominus'}$ is formal potential of an electrode, V; R is the gas constant, 8.314 J K^{-1} mol^{-1}; T is temperature, K; F is the Faraday constant, 96 485 C mol^{-1}; D is diffusion coefficient, m^2 s^{-1}; α is the transfer coefficient; v is scan rate, V s^{-1}. Thus, the plot of E_p *vs.* $\ln v^{1/2}$ determined at different scan rates should have linear dependence with a slope of $-RT/\alpha F$, from which the value of transfer coefficient α can be determined. Fig. 3 shows the E_p *vs.* $\ln v^{1/2}$ extracted from Fig. 2, it is evident that E_p decreases with the increase of $\ln v^{1/2}$ exhibiting linear dependence. Using linear fitting, a straight line (the red line in Fig. 3) with the correlation coefficient reaching 0.99 is obtained, with a slop of -0.063, which then is substituted into eqn (1), obtaining value of transfer coefficient $\alpha = 0.45$.

Similarly, for irreversible electrode reaction the following equation is used to determine the relationship between I_p and square root of the scan rates $v^{1/2}$:[37,38]

$$I_p = -0.4958nFD^{\frac{1}{2}}AC^*\left(\frac{\alpha F}{RT}\right)^{\frac{1}{2}}v^{1/2} \quad (2)$$

where n is stoichiometric number of electrons in the electrode reaction; A is the electrode area, m^2; C^* is the concentration of Ni^{2+}, mol cm^{-3}. Eqn (2) illustrates that I_p is proportional to the square root of the scan rates and the slop should be $-0.4958nFD^{\frac{1}{2}}AC^*\left(\frac{\alpha F}{RT}\right)^{\frac{1}{2}}$. As the value of transfer coefficient α is already determined, the value of diffusion coefficient D can be calculated by liner fitting the curve I_p *vs.* $v^{1/2}$. Fig. 4 presents the plot of current peak I_p *versus* scan rate $v^{1/2}$ and the fitted curve. Substituting the value of α into eqn (2), the value of the diffusion coefficient D 5.27 $\times$ 10^{-10} m^2 s^{-1} is obtained, which is slightly lower than the reported values. Thus, in the ionic liquid used for present study, the diffusion of Ni^{2+} is the limitation process for electrodeposition.

The development of Ni grains during electrodeposition

In order to understand the nucleation and growth of nickel crystal grains, the grain size and population density on coatings at different stages of electrodeposition were characterized. Fig. 5(a–c) present the SEM images of Ni coatings deposited on copper substrate under potentiostatic deposition at -0.6 V (*vs.* Ag) in IL with water concentration of 15 wt% at 363 K. It is evident that spherical grains with different grain size nucleated and progressively developed on the surface of copper substrate. As reported by Benjamin Scharifker formation of spherical grains is the result of diffusion limited growth.[39,40] The histogram of grain size (measured by ImageJ software) and population density is shown in Fig. 5(d). Apparently, the distributions of the grain size are closed to the Gaussian distribution, which are characterized by the mean sizes of 10 nm, 54 nm and 57 nm for coatings formed with a total deposition capacity of 0.04 mA h cm^{-2}, 0.08 mA h cm^{-2} and

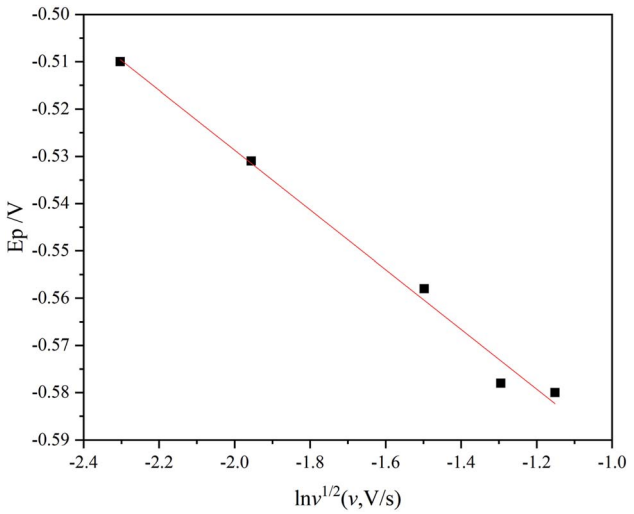

Fig. 3 Plot of peak potential against natural logarithm of the square root of scan rate.

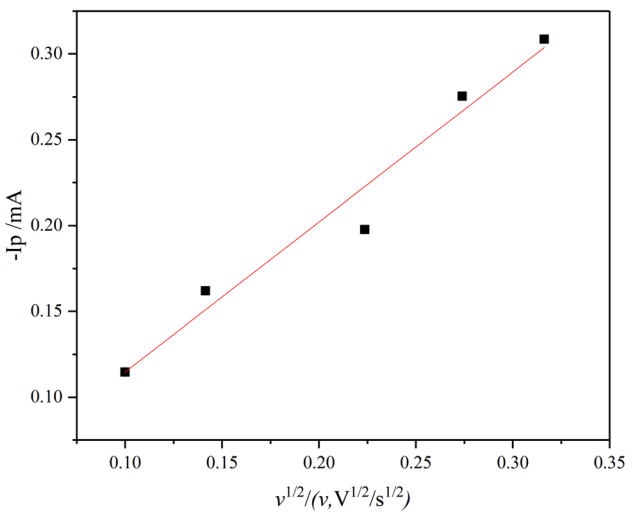

Fig. 4 Cathodic peak current of cyclic voltammograms at 333 K under different scan rates.

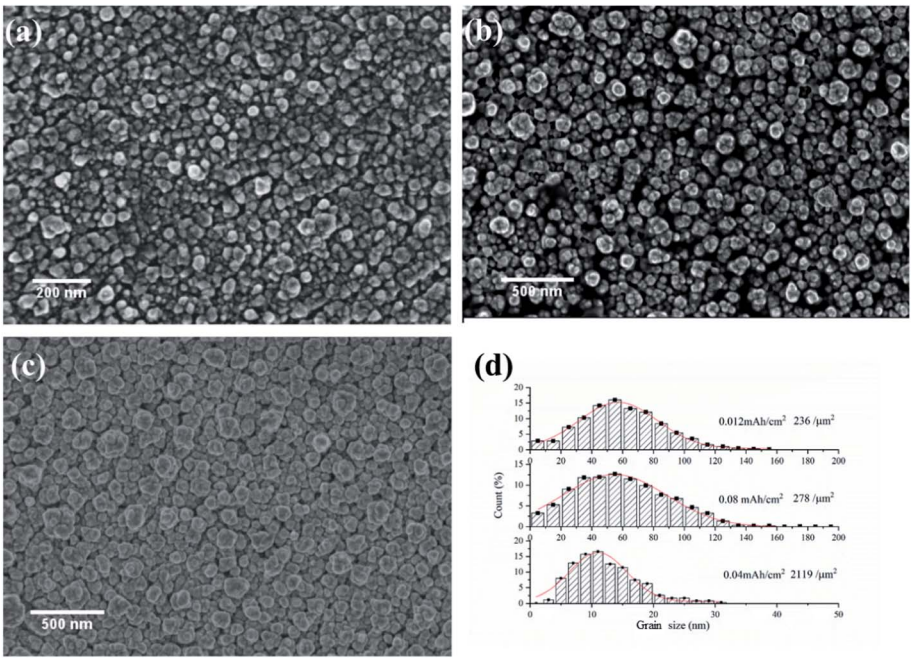

Fig. 5 (a–c) SEM images of Ni coatings formed on copper substrate under potentiostatic deposition at −0.6 V (*vs.* Ag) and 363 K for a total capacity of 0.04 mA h cm^{-2}, 0.08 mA h cm^{-2} and 0.12 mA h cm^{-2} respectively. (d) Histogram of grain size obtained from (a–c).

0.12 mA h cm^{-2} respectively (equivalent to 50 nm, 100 nm and 150 nm of nickel coating). The grain population density for the three conditions are 2119, 278 and 236 per square micron respectively. The lognormal distribution of grain size is commonly observed in various crystallization processes especially in Kolmogorov–Avrami–Mehl–Johnson (KAMJ) random nucleation and growth (RNG) processes.[40] KAMJ mode assumes that nuclei are randomly distributed with independently growth rate, and the growth cease where two particles impinge. Thus, the nucleation process of nickel in [BMIM][DBP] can be descripted as follows. At initial stage, nuclei form on the surface of the electrode with high population density. Each grain grows independently until impinges on other growing grains at which point the grains stop growing laterally. Then, electrodeposition progress steadily with a constant growth rate, and the grain size and population density of grains remain unchanged, which is consistent with the model describe in previous work.[40,41]

The influence of electrodeposition voltage

Fig. 6 shows the SEM images of the nickel coatings obtained at 363 K by potentiostatic electrodeposition with various voltages for 1 h. The coating obtained at −0.4 V (*vs.* Ag) is uniform and compact, as displayed in Fig. 6(a). For the coating formed at −0.5 V (*vs.* Ag), the surface is less uniform, exhibiting cracks and protuberances. When a voltage of −0.6 V (*vs.* Ag) was applied, as shown in Fig. 6(c), many small spherical particles are present on the surface. Fig. 6(d) presents the coating obtained at a potential voltage of −0.7 V (*vs.* Ag), exhibiting rough surface with many larger spherical particles compared with Fig. 6(c).

At low overpotential, deposition rate is determined by the reduction reaction rate; the growth of Ni crystal is relatively slow resulting in relatively fine grains and uniform coatings. When relatively larger overpotential is applied, deposition rate is relatively high and is determined by diffusion process, resulting in relatively large grains and development of protuberances crystal on coating surface.[30,42,43] Therefore, overpotential has significant influence on the morphology of resultant coatings.

The crystal structure of the Ni coating obtained at −0.6 V (*vs.* Ag) in 1.0 M $NiCl_2 \cdot 6H_2O$/[BMIM][DBP] at 363 K for 2 hours was characterized by XRD (Fig. 7). It is evident that there are three characteristic diffraction peaks at 2θ of 43.29°, 50.43° and 74.09°, which are related to (111), (200) and (220) planes of nickel crystal (JCPDS no. 01-070-1849) respectively. In most reported works the strongest diffraction peak of electrodeposited Ni coating comes from Ni (111), indicating randomly distributed grains (JCPDS no. 01-070-1849).[25,30,31,38] However, it is evident that in Fig. 6 that the strongest diffraction peak of the coating formed in [BMIM][DBP] comes from Ni (220), and that the peak intensity ratio of $I_{(220)}/I_{(111)}$ reaches 11.27 whereas this value is around 0.21 in most reported works.[25,30,31,38] Thus, XRD indicates that nickel crystal formed in [BMIM][DBP] has preferential growth orientations.

Influence of water content in IL

In water- and air- stable ILs, dissolving of water is inevitable. In previous work, some researchers noticed that the dissolution of molecule solvent in ILs has significant influence on the physical properties of ILs.[44]

In order to investigate the influence of dissolved water in the IL on the microstructure of the resultant coatings, electrodeposition was conducted in the IL at 363 K with water concentrations of 5 wt%, 10 wt%, 20 wt% and 30 wt% under potentiostatic deposition at −0.6 V (*vs.* Ag) with total capacity of 0.08 mA h cm^{-2}. At very low water concentration (Fig. 8(a)),

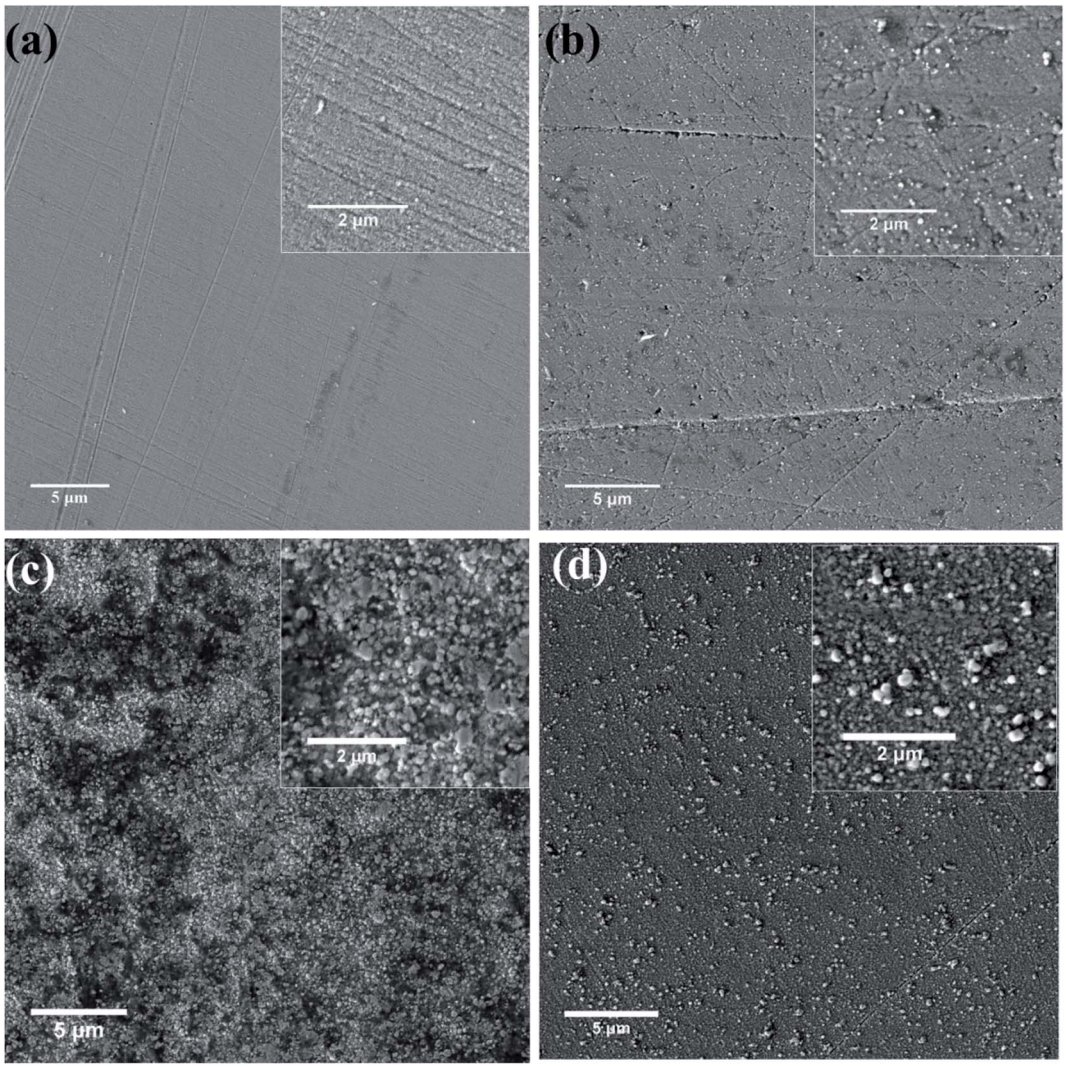

Fig. 6 SEM images of nickel coatings formed on copper substrate at 363 K under potentiostatic electrodeposition at various potential (*vs.* Ag) (a) −0.40, (b) −0.50, (c) −0.60, (d) −0.70.

edges and steps are formed on the surface indicating two-dimensional growth. Increasing water concentration to 10 wt%, edges and steps are still present on coating surface, with some spherical particles also being spotted. However, at higher water concentration the surface morphology is significantly different, as shown in Fig. 8(c), exhibiting fine grains on coating surface. When water concentration reaches 30 wt%, cracks can be seen on coating surface, as revealed in Fig. 8(d).

Fig. 8 shows clearly that water content in the IL affects the electrodeposition process. At very low water concentration, nickel mainly grows layer by layer, following two-dimensional growth. With increasing water concentration, the deposition process gradually changes to three-dimensional growth. Moreover, electrodeposition in IL with high water concentration results in fine grains, while high water concentration also brings about cracks. It is shown in previous study that water content in the IL [BMIM][DBP] reduces the viscosity of the solution, and also results in a drop of pH value.[33] Lower viscosity is beneficial to ionic migration, therefore, fine grains are formed in the IL with higher water concentration. However, low pH value means high concentration of H^+, which leads to hydrogen evolution and, consequently, cracks in the coatings.

The surface topography of the nickel coatings obtained in IL with various water concentration were also characterized using Keyence X200K 3D laser microscope equipped with VK-H1XMC multi-file analysis software. The 3D images are shown in Fig. 9. The surface roughness obtained from the VK-H1XMC multi-file analysis software is presented in Table 1. Fig. 9(a) and (b) show that at low water concentration the surfaces of the resultant coatings are relatively rough with many particles. The R_a are 0.36 ± 0.02 μm and 0.23 ± 0.01 μm for coatings formed in IL with 5 wt% and 10 wt% water concentration respectively. Fig. 9(c) and (d) show the 3D surface images of the coatings obtained in the IL with water concentration of 20 wt% and 30 wt%. It is evident that the surfaces are very smooth with R_a value of 0.034 ± 0.01 μm and 0.04 ± 0.01 μm respectively. Thus, water content in the IL promotes the formation of smooth and uniform coatings.

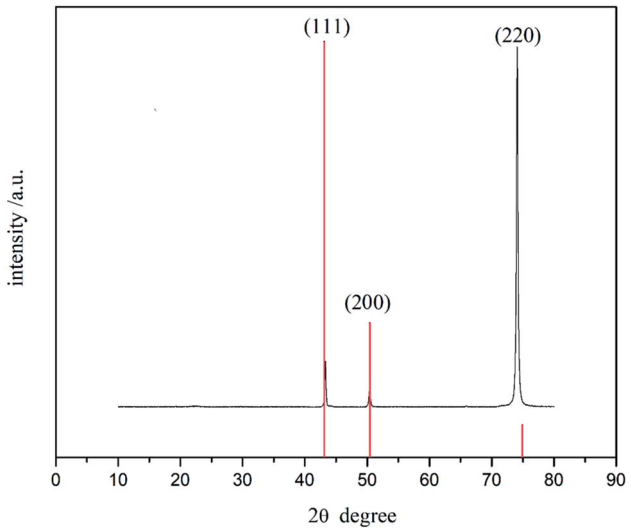

Fig. 7 XRD pattern of the nickel coating obtained by potentiostatic electrodeposition.

The mechanism of Ni^{2+} reduction in ionic liquid

In order to determine the state of nickel in the IL, electrospray ionization mass spectrometry (ESI-MS) was employed to analyses both pure IL and IL containing $NiCl_2$. In the positive-ion mode, the peak of $m/z = 486.9$ is the strongest peak, followed by peaks of $m/z = 1182.6$, 1530.5, 1740.4 and 1392. The peak of $m/z = 486.9$ comes from $\{[BMIM]_2[DBP]_1\}^+$ and $\{[BMIM]_4[DBP]_2\}^{2+}$; $m/z = 1182.6$, 1530.5, 1740.4 and 1392 correspond to $\{[BMIM]_4[DBP]_3\}^+$ $\{[BMIM]_5[DBP]_4\}^+$ and $\{[BMIM]_5[DBP]_5\}^+$ respectively.[44] The peak for parent cation $[BMIM]^+$ can be found at $m/z = 139.1$ with relatively low intensity. Similarly, for the negative-ion model, the intensity of the parent anion $[DBP]^-$ is also very low, and the strongest peaks of m/z correspond to $\{[BMIM]_2[DBP]_3\}^-$, $\{[BMIM]_4[DBP]_6\}^{2-}$, $\{[BMIM]_4[DBP]_6\}^{2-}$, $\{[BMIM]_3[DBP]_4\}^-$ and $\{[BMIM]_4[DBP]_5\}^-$. Thus, it is evident that several parent cations and anions aggregate with each other in the IL.[45] The ESI-MS of the IL containing $NiCl_2$ shows similar result as the pure IL except for three new positive ion peaks at $m/z = 963$, 1137 and 1311, corresponding to {Ni

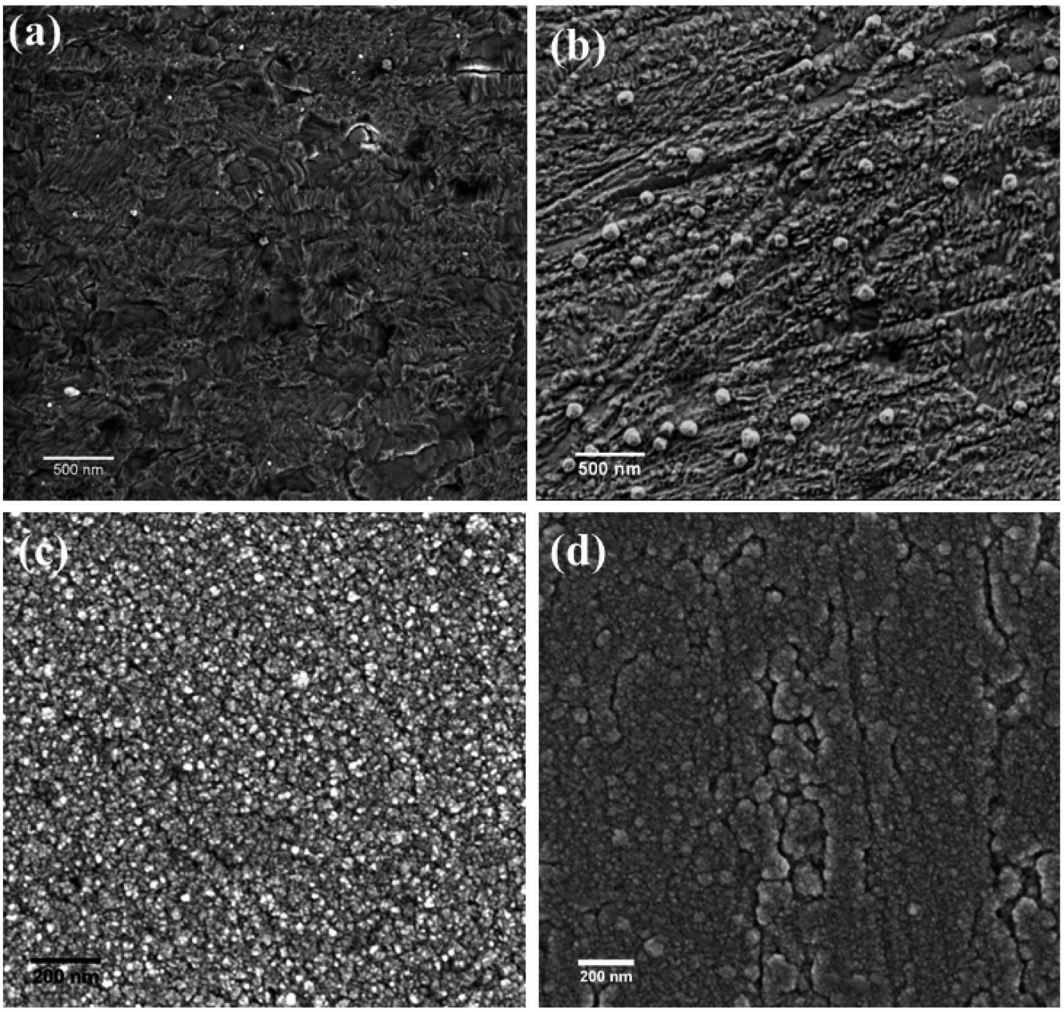

Fig. 8 SEM images showing the surface morphology of the coatings obtained deposited in the IL with various water concentration: (a) 5 wt%, (b) 10 wt%, (c) 20 wt%, (d) 30 wt%. Electrodeposition obtained deposited were conducted under potentiostatic deposition at −0.6 V (*vs.* Ag) for a total capacity of 0.08 mA h cm^{-2}.

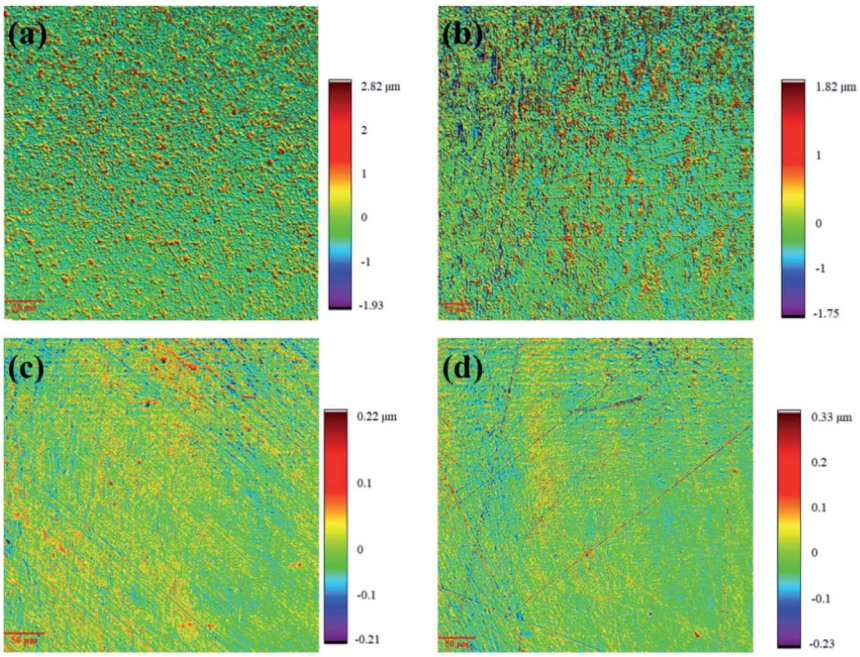

Fig. 9 Surface topography of the nickel coating electrodeposited in IL with different water concentration at 363 K: (a) 5 wt%, (b) 10 wt%, (c) 20 wt%, (d) 30 wt%.

Table 1 Surface roughness of the coatings obtained in IL with various water concentrations

Water concentration	5 wt%	10 wt%	20 wt%	30 wt%
R_a (μm)	0.36 ± 0.02	0.23 ± 0.01	0.03 ± 0.01	0.04 ± 0.01

$[BMIM]_3[DBP]_2Cl_2\}^+$, $\{Ni[BMIM]_3[DBP]_3Cl\}^+$ and $\{Ni[BMIM]_4[DBP]_3Cl_2\}^+$ respectively. Thus, nickel ions form complexes with the cluster parent cations and anions in this IL.[45–47]

Therefore, the reduction of Ni^{2+} can be described as follows: firstly, the complexes containing nickel ions ($\{Ni[BMIM]_x[DBP]_yCl_z\}^{(2+x-y-z)+}$) in the solution was absorbed on the surface of the substrate; then, under applied overpotential, nickel ion obtained two electrons to form a nickel atom.

Conclusions

In this study, nickel coatings were obtained by electrodeposition in a water- and air- stable 1-butyl-3-methylimidazolium dibutylphosphate ([BMIM][DBP]) ionic liquid. The electrodeposition of nickel in [BMIM][DBP] is an irreversible electrochemical process. The diffusion of Ni^{2+} is a rate-determining step. The diffusion coefficient of Ni^{2+}, determined by cyclic voltammetry, is 5.27×10^{-10} m^2 s^{-1}. Water content in the IL and applied overpotential have significant influence on the morphology of the resultant coatings. Water in the IL promoted the formation of uniform coating and enhance hydrogen evolution. Low overpotential resulted in relative smooth coating surface while high overpotential increased coating surface roughness.

Conflicts of interest

There are no conflicts to declare.

Acknowledgements

The authors gratefully acknowledge the support by China Scholarship Council.

References

1 J. S. Wilkes, P. Wasserscheid and T. Welton, *Ionic liquids in synthesis*, John Wiley & Sons, Weinheim, 2008, pp. 1–6.
2 R. D. Rogers and K. R. Seddon, *Science*, 2003, **302**, 792–793.
3 Q. Zhang, Q. Wang, S. Zhang, X. Lu and X. Zhang, *ChemPhysChem*, 2016, **17**, 335–351.
4 G. E. Gray, P. A. Kohl and J. Winnick, *J. Electrochem. Soc.*, 1995, **142**, 3636–3642.
5 M. Galiński, A. Lewandowski and I. Stępniak, *Electrochim. Acta*, 2006, **51**, 5567–5580.
6 T. Torimoto, T. Tsuda, K. Okazaki and S. Kuwabata, *Adv. Mater.*, 2010, **22**, 1196–1221.
7 Y. L. Zhu, Y. Katayama and T. Miura, *J. Electrochem. Soc.*, 2012, **159**, D699–D704.
8 Y. L. Zhu, Y. Katayama and T. Miura, *Electrochem. Solid-State Lett.*, 2011, **14**, D110–D115.
9 Y. Katayama, R. Fukui and T. Miura, *Electrochemistry*, 2013, **81**, 532–534.
10 R. Fukui, Y. Katayama and T. Miura, *Electrochim. Acta*, 2011, **56**, 1190–1196.
11 M. H. Allahyarzadeh, B. Roozbehani and A. Ashrafi, *Electrochim. Acta*, 2011, **56**, 10210–10216.

12 Y. T. Hsieh, M. C. Lai, H. L. Huang and I. W. Sun, *Electrochim. Acta*, 2014, **117**, 217–223.
13 M. Li, Z. W. Wang and R. G. Reddy, *Electrochim. Acta*, 2014, **123**, 325–331.
14 W. Sun, X. Q. Li, P. Qin and K. Jiao, *J. Phys. Chem. C*, 2009, **113**, 11294–11300.
15 T. M. Liu, R. Vilar, S. Eugenio, J. Grondin and Y. Danten, *J. Appl. Electrochem.*, 2015, **45**, 87–93.
16 S. Z. El Abedin, A. Y. Saad, H. K. Farag, N. Borisenko, Q. X. Liu and F. Endres, *Electrochim. Acta*, 2007, **52**, 2746–2754.
17 N. R. Brooks, S. Schaltin, K. Van Hecke, L. Van Meervelt, K. Binnemans and J. Fransaer, *Chem.–Eur. J.*, 2011, **17**, 5054–5059.
18 S. Caporali, P. Marcantelli, C. Chiappe and C. S. Pomelli, *Surf. Coat. Technol.*, 2015, **264**, 23–31.
19 W. Dobbs, J. M. Suisse, L. Douce and R. Welter, *Angew. Chem.*, 2006, **45**, 4179–4182.
20 A. P. Abbott, F. Qiu, H. M. A. Abood, M. R. Ali and K. S. Ryder, *Phys. Chem. Chem. Phys.*, 2010, **12**, 1862–1872.
21 A. Bakkar and V. Neubert, *Electrochem. Commun.*, 2015, **51**, 113–116.
22 J. Tang and K. Azumi, *Electrochim. Acta*, 2011, **56**, 1130–1137.
23 A. V. Oriani, P. Cojocaru, C. Monzani, E. Valles and E. Gomez, *J. Electroanal. Chem.*, 2017, **793**, 85–92.
24 S. Z. El Abedin, P. Giridhar, P. Schwab and F. Endres, *Electrochem. Commun.*, 2010, **12**, 1084–1086.
25 A. P. Abbott, A. Ballantyne, R. C. Harris, J. A. Juma, K. S. Ryder and G. Forrest, *Electrochim. Acta*, 2015, **176**, 718–726.
26 A. P. Abbott, A. Ballantyne, R. C. Harris, J. A. Juma and K. S. Ryder, *Phys. Chem. Chem. Phys.*, 2017, **19**, 3219–3231.
27 J. X. Li, H. Lai, B. Q. Fan, B. Zhuang, L. H. Guan and Z. G. Huang, *J. Alloys Compd.*, 2009, **477**, 547–551.
28 O. P. Watts, *Trans. Am. Electrochem. Soc.*, 1916, **29**, 395–403.
29 J. P. Hoare, *J. Electrochem. Soc.*, 1986, **133**, C322.
30 M.-J. Deng, I. W. Sun, P.-Y. Chen, J.-K. Chang and W.-T. Tsai, *Electrochim. Acta*, 2008, **53**, 5812–5818.
31 Y.-L. Zhu, Y. Kozuma, Y. Katayama and T. Miura, *Electrochim. Acta*, 2009, **54**, 7502–7506.
32 B. Meenatchi, V. Renuga and A. Manikandan, *J. Inorg. Organomet. Polym.*, 2016, **26**, 423–430.
33 Y. Zheng, R. Peng, H. Jin, Y. Luo and Y. Ping, *Surf. Coat. Technol.*, 2017, **325**, 539–547.
34 C. H. Hamann, A. Hamnett and W. Vielstich, *Electrochemistry*, Wiley-VCH, Weinheim, 2007, pp. 118–136.
35 D. K. Gosser, *Cyclic voltammetry: simulation and analysis of reaction mechanisms*, Wiley-VCH, New York, 1993, pp. 1–24.
36 W. H. Reinmuth, *Anal. Chem.*, 1960, **32**, 1891–1892.
37 A. J. Bard and L. R. Faulkner, *Electrochemical Methods: Fundamentals and Applications*, John Wiley & Sons, New York, 2000, pp. 235–237.
38 M. Li, Z. Wang and R. G. Reddy, *J. Electrochem. Soc.*, 2014, **161**, D150–D153.
39 R. B. Bergmann and A. Bill, *J. Cryst. Growth*, 2008, **310**, 3135–3138.
40 A. V. Teran, A. Bill and R. B. Bergmann, *Phys. Rev. B: Condens. Matter Mater. Phys.*, 2010, **81**, 075319.
41 M. Tian, J. Wang, J. Kurtz, T. E. Mallouk and M. H. Chan, *Nano Lett.*, 2003, **3**, 919–923.
42 S. Wang, X. Zou, Y. Lu, S. Rao, X. Xie, Z. Pang, X. Lu, Q. Xu and Z. Zhou, *Int. J. Hydrogen Energy*, 2018, **43**, 15673–15686.
43 L. Guo and P. C. Searson, *Electrochim. Acta*, 2010, **55**, 4086–4091.
44 L. S. Bobrova, F. I. Danilov and V. S. Protsenko, *J. Mol. Liq.*, 2016, **223**, 48–53.
45 Z. B. Alfassi, R. E. Huie, B. L. Milman and P. Neta, *Anal. Bioanal. Chem.*, 2003, **377**, 159–164.
46 S. Kitaoka, K. Nobuoka, Y. Ishikawa and A. Wakisaka, *Anal. Sci.*, 2008, **24**, 1311–1314.
47 B. L. Milman and Z. B. Alfassi, *Eur. J. Mass Spectrom.*, 2017, **11**, 35–42.